IBRACON Structures and Materials Journal
Revista IBRACON de Estruturas e Materiais

ORIGINAL ARTICLE

Experimental results and limit load analysis by the strut-and-tie method (STM) in deep beams with notches and openings

Resultados experimentais e análise de carga limite pelo Método de Bielas e Tirantes (MBT) de vigas-parede com entalhes e aberturas

Izabel Castro de Abreu Neta[a]

Antonio Carlos de Oliveira Miranda[a]

Rodrigo de Melo Lameiras[a]

Carlos Henrique de Oliveira Leite[a]

[a]Universidade de Brasília – UNB, Departamento de Engenharia Civil e Ambiental, Brasília, DF, Brasil

Abstract: This article presents experimental results of eight non-aligned, non-geometrically symmetrical deep beams with notches and openings. The variables considered in the study were the presence of web reinforcement, and the geometry of the deep beams. Along with the experimental investigation, a study of strut-and-tie models (STM) representing the behavior (failure mode and maximum load) of reinforced concrete deep beams with complex geometries was performed. The experimental results showed that the ultimate load capacity of deep beams is significantly affected by the presence of reinforcement in the web. Furthermore, the study showed that the STM is conservative and tends to underestimate the results, reducing its ability to predict failure load.

Keywords: deep beams, notches and openings, complex geometries, strut-and-tie models, conservative.

Resumo: Esse trabalho apresenta resultados experimentais de oito vigas-parede com entalhes e furos, não alinhados e não simétricos geometricamente. As variáveis consideradas no estudo foram a presença de armadura na alma ou não, e a geometria das vigas-parede. Junto com a investigação experimental, foi realizado um estudo de modelos de bielas e tirantes (MBT) que representassem o comportamento (modo de falha e carga máxima) das vigas-parede de concreto armado com geometrias complexas. Os resultados experimentais mostraram que a capacidade de carga última das vigas-parede é afetada significativamente pela existência de armadura na alma. Além disso, o estudo mostrou que o MBT é conservador, e tende a subestimar os resultados, reduzindo a sua capacidade de predição de carga de falha.

Palavras-chave: vigas-parede, entales e aberturas, geometrias complexas, modelo de bielas e tirantes, conservador.

1 INTRODUCTION

The technical and scientific advances in the construction industry have led to the design of structures that are increasingly daring and different from the usual. Structural engineers are required to design structural elements with geometric variations in sections in order to meet the criteria of architectural and installation projects. These elements contain "D" (discontinuity) regions that are not compatible with traditional methods of design critical sections. The structural elements that work in this context include beams and deep beams with geometric discontinuities.

According to NBR 6118 [1], deep beams are different from slender beams in that they have a span-to-depth ratio of less than 2 for simply supported beams, and less than 3 for continuous beams. They are utilized for offshore structures, retaining walls, reservoirs, transition structures, and on the facades of tall buildings [2]–[4].

Meeting the requirements of utility design often results in openings being created in the web of deep beams. These openings are typically made to accommodate services such as ventilation ducts, air conditioning, water supply, electricity, and telecommunications. However, these openings can weaken the beams' strength in comparison to their solid counterparts, especially if the opening interrupts the concrete strut. Additionally, stress is redirected due to the reduction of the cross-sectional area, which concentrates in the corners of the openings. This causes a drastic reduction in the beam's final strength, leading to deflections and cracks. This reduction in the ultimate strength of beams has been documented by [5]–[11].

In recent years, several experimental studies have been conducted to evaluate the behavior of deep beams with openings in the web [8], [12]–[26]. Various issues and discussions have been addressed regarding their performance as the zones of geometric discontinuities significantly affect the structural behavior, introducing disturbances in the strain field of the element, leading to a more complex problem. Most of these studies involve the analysis of deep beams with circular, square, and rectangular openings [8], [12]–[26].

The analysis of reinforced concrete deep beams does not follow the same stress behavior as slender beams, and the presence of openings in the web aggravates the situation further. One way to evaluate and design deep beams is through the Strut-and-Tie Model (STM), which is a useful tool for designing complex or unusual reinforced concrete members. This model is recommended by standards such as ACI 318 [27], Eurocode 2 [28], Fib [29], NBR 6118 [1], among others.

The strut-and-tie Model (STM) was introduced by Schlaich et al. [30] and is based on the classical truss analogy of Mörsch [31] and Ritter [32]. This model aims to express complex stress patterns based on the path of efforts in the structural element. Concrete struts carry compressive stresses, while ties, which represent the reinforcement, resist to tensile stresses. The STM is based on the Lower Limit of Plasticity Theory, which ensures equilibrium and requires that the structural element has enough ductility so that the struts and ties can develop. According to Fan et al. [33], despite the applications of STM in structural design, there is a need for more guidelines and reports on STM geometry in practice.

Developing an ideal, accurate, and coherent strut-and-tie Model (STM) is not only the main responsibility of designing concrete structures using this method but also a better option for planning concrete structures. It should be noted that more than one admissible STM can be created for a given geometry and load case. Designers may create different ideal STM and develop significantly different reinforcements for the same structural member. Selecting an ideal STM is challenging for structural engineers, especially when developing projects containing deep beams with complex geometries, as it requires subjective experience from the designer.

The objective of this study is to experimentally assess the behavior of deep beams with complex geometries, with notch and non-aligned and asymmetrically diamond-shaped openings. This may cause discontinuity in the ties and disrupt the formation of compression struts. Additionally, this study aims to build strut-and-tie models to predict failure modes and maximum loads. By doing so, it will increase the number of experimental investigations on deep beams with unconventional geometries and strut-and-tie model (STM) analysis.

2 EXPERIMENTAL PROGRAM

The experimental program consisted of tests on eight reinforced concrete deep beams with a cross-section of 140 mm in width and 700 mm in depth, and a 1000 mm span. The variables studied were the presence or absence of web reinforcement and the deep beam geometry.

The deep beams investigated in the study had two distinct geometries, as shown in Figure 1. The first one, DB-H1, included a notch in the lower part of the model, creating a discontinuity in the tie and an asymmetric diamond-shaped opening on the right side, disrupting the load path connecting the support to the load application point. This opening was also not aligned with the external geometry, as depicted in Figure 1(a). The DB-H2 geometry, illustrated in Figure 1(b), followed the same concept as the first, but with the addition of a diamond-shaped opening on the left side, further complicating the introduction of a compression strut by disrupting the load path on that side.
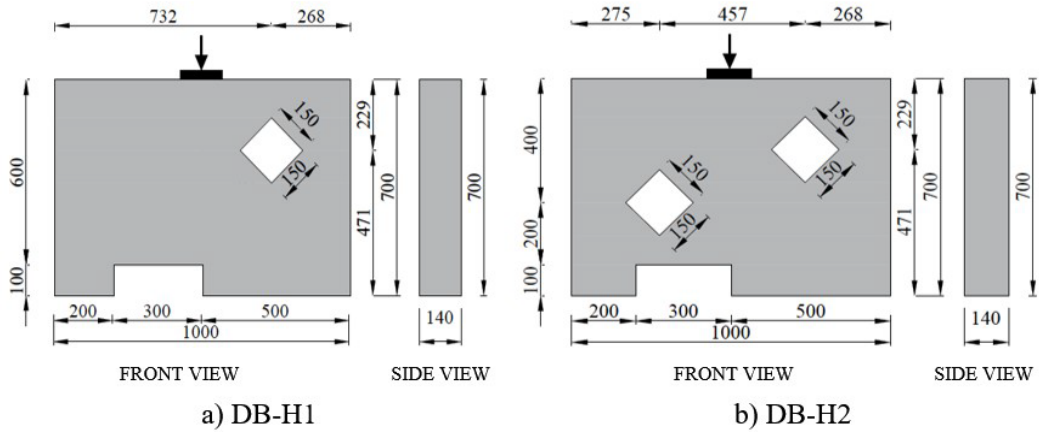
Figure 1. Deep beam geometries (dimensions in mm)

Table 1 summarizes the tested geometries. Models with and without web reinforcement were created for each geometry shown in Figure 1, with two samples each. The notation used is: DB for Deep Beam; NR for no reinforcement in the web, and WR for the presence of reinforcement in the web. H1 and H2 indicate the number of diamond-shaped openings in the web.

Table 1. Deep beam details

Deep Beams	L (mm)	h (mm)	b (mm)	L/h
DB-NR-H1-1				
DB-NR-H1-2				
DB-WR-H1-1				
DB-WR-H1-2	1000	700	140	1.43
DB-NR-H2-1				
DB-NR-H2-2				
DB-WR-H2-1				
DB-WR-H2-2				

2.1 Details of the reinforcements

The flexural and transverse reinforcement in the tested deep beams consisted of CA-50 type steel bars, where CA stands for Reinforced Concrete and the value 50 corresponds to the characteristic yield strength of steel, meaning that the CA-50 steel bars must have a characteristic yield strength of 500 MPa. A cover of 25 mm was used in all models to ensure adequate reinforcement. Figures 2 to 5 provide detailed information on the reinforcement used in the tested deep beams.
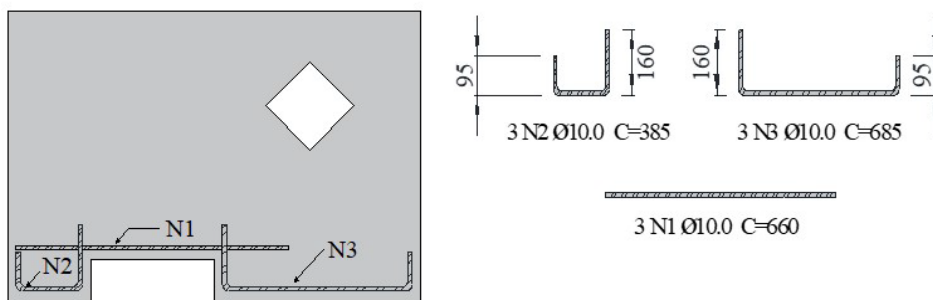

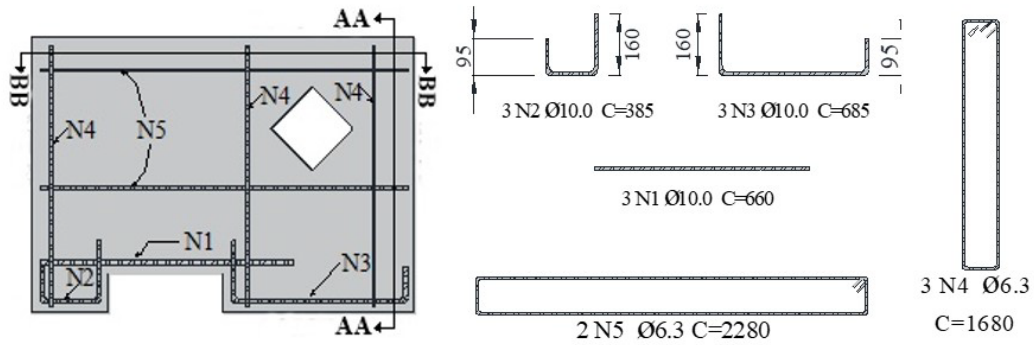**Figure 2.** Details of reinforcements on DB-NR-H1 (dimensions in mm)

Rev. IBRACON Estrut. Mater., vol. 17, no. 6, e17606, 2024

3/21

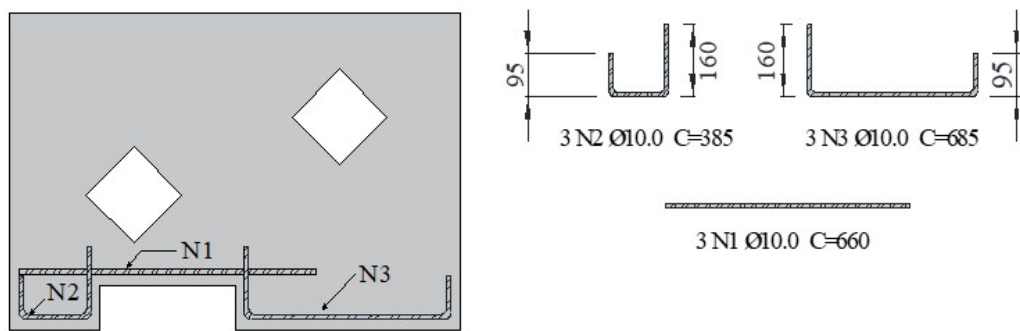**Figure 3.** Details of reinforcements on DB-WR-H1 (dimensions in mm)

Figure 4. Details of reinforcements on DB-NR-H2 (dimensions in mm)
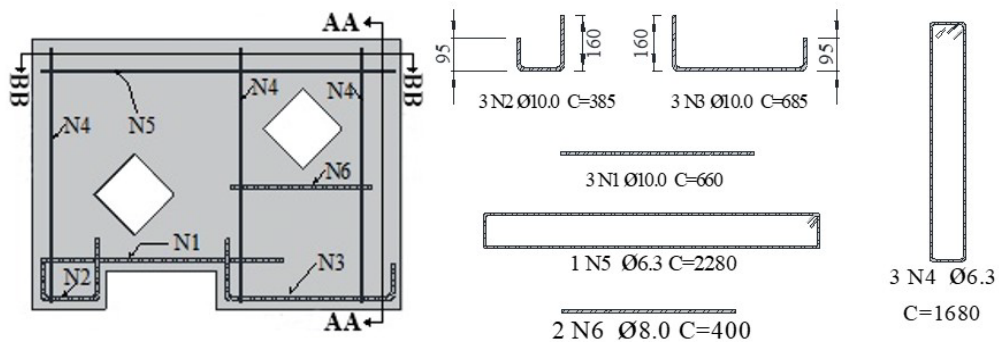

Figure 5. Details of reinforcements on DB-WR-H2 (dimensions in mm)

2.2 Materials Properties

To compare the results, the properties of the materials used to produce the deep beams, i.e., concrete and steel, were tested in the laboratory. Cylindrical specimens were prepared during the construction of the deep beams to verify the mechanical properties of the concrete, following the recommendations of NBR 5738 [34]. Compression tests were carried out based on NBR 5739 [35], and tensile tests were performed following the recommendations of NBR 7222 [36]. Table 2 summarizes the mechanical properties of the concrete used in the research.

Rev. IBRACON Estrut. Mater., vol. 17, no. 6, e17606, 2024

4/21

Table 2. Mechanical properties of concrete

Age	f_c (MPa)	$f_{c, average}$ (MPa)	E_c (GPa)	$E_{c, average}$ (GPa)	$f_{ct,sp}$ (MPa)	$f_{ct,sp\ average}$ (MPa)
	42.72		38.17		4.3	
	47.74					
145th day	50.30	47.64	40.80	38.99	3.3	3.7
	47.49					
	49.96		37.99		3.5	

Three specimens of each diameter were tested under tension to evaluate the mechanical properties of the steel used for reinforcement, following the recommendations of NBR 6892 [37]. Table 3 presents the mechanical properties of the steel bars used to reinforce the beams.

Table 3. Mechanical properties of the reinforcement

Ø (mm)	f_{ys} (MPa)	ε_{ys} (‰)	E_s (GPa)
6.3	594	2.88	206
8.0	614	3.04	202
10.0	551	2.87	192

2.3 Instrumentation

To measure the strain of the flexural reinforcement of the beams, two diametrically opposed electrical strain gauges were used on the central bar of the N1 flexural reinforcement, located at the reentrant corner in the middle of the span.

2.4 Test Setup

The configuration of the tests is shown schematically in Figure 6. In this test system, the beams were positioned in the reaction frame on two support devices, consisting of steel plates measuring 140×140×40 mm and solid steel cylinders with a diameter of 25.4 mm.
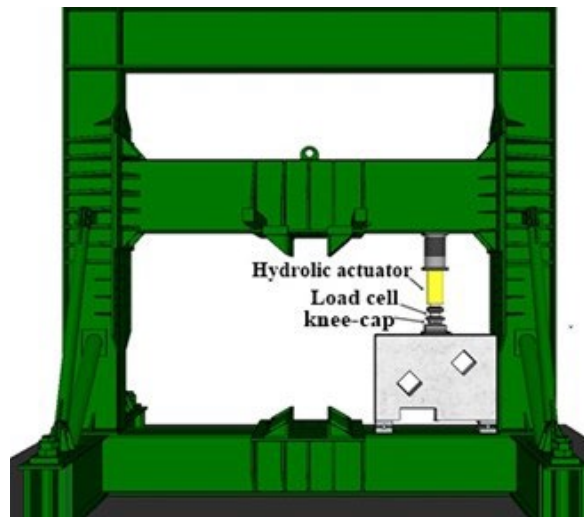

Figure 6. Test setup.

The deep beams were subjected to three-point flexural failure tests. The load application system consisted of a 500 kN capacity load cell and a hydraulic actuator installed in line with the cell. The load was applied through a hydraulic actuator, transmitted to the model by a steel plate measuring 140×140×40 mm, and a hinge was used to minimize possible eccentricities.

Rev. IBRACON Estrut. Mater., vol. 17, no. 6, e17606, 2024

5/21

3 EXPERIMENTAL RESULTS AND DISCUSSIONS

3.1 Cracking Load, Failure Load and Failure Modes

The initial results, which include the cracking load, failure load, and failure modes of the deep beams, are summarized in Table 4. The cracking load was determined through visual inspection.

As shown in Table 4 and Figure 7, the presence of web reinforcement has a significant impact on the ultimate load capacity of the deep beams. Deep beams with web reinforcement presented higher strength and ductility when compared to those without reinforcement, showing that stirrups contribute to an increase in shear strength. The presence of numerous cracks prior to failure allowed for a significant redistribution of forces.

Regarding the average failure loads of deep beams with one opening and without web reinforcement (DB-NR-H1-1 and DB-NR-H1-2), beams DB-WR-H1-1 and DB-WR-H1-2 containing reinforcement showed an average increase in strength of around 103.31% in comparison to those without reinforcement in the web. As for the comparison of the average failure loads of deep beams with two openings, beams DB-WR-H2-1 and DB-WR-H2-2 with web reinforcement showed an average increase in strength of about 31.4% compared to deep beams DB-NR-H2-1 and DB-NR-H2-2 without reinforcement.

Deep beams with lower ultimate strength (without web reinforcement) had higher ratios between cracking load and failure load when compared to beams with higher ultimate strength (with web reinforcement). This can be seen in Table 4 and Figure 8.

The deep beams DB-WR-H1-1 and DB-WR-H1-2 showed significant differences in failure loads. This behavior likely occurred due to inadequate compaction during the concreting of DB-WR-H1-2, reducing its performance and altering its resistance mechanism. Consequently, it exhibited a lower load-carrying capacity.

Table 4. Experimental results: cracking load, failure load and failure modes

Deep Beams	P_c (kN)	P_f (kN)	$P_{f,average}$ (kN)	P_c/P_f (%)	Failure Modes
DB-NR-H1-1	159.00	193.68	200.67	82.09	Shear failure and anchorage failure
DB-NR-H1-2	186.00	207.66		89.57	
DB-WR-H1-1	160.00	474.90	407.99	33.69	Flexural failure
DB-WR-H1-2	199.00	341.07		58.34	
DB-NR-H2-1	133.00	210.12	233.74	63.30	Shear failure and anchorage failure
DB-NR-H2-2	133.00	257.37		51.67	
DB-WR-H2-1	150.00	305.61	307.07	49.08	Flexural-Shear failure
DB-WR-H2-2	117.00	308.52		37.92	

P_c = First visual cracking load; P_f = Failure Load

(a) Beams with an opening in the web.   (b) Beams with two openings in the web.
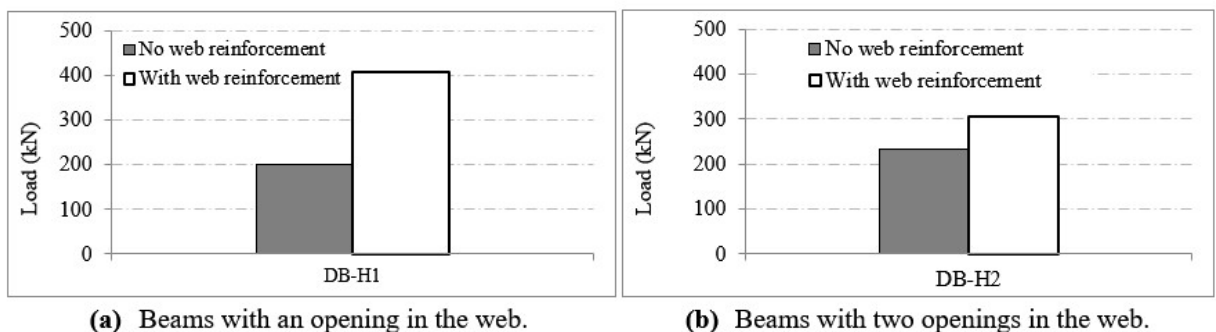
Figure 7. Comparison of average failure loads

Rev. IBRACON Estrut. Mater., vol. 17, no. 6, e17606, 2024

6/21

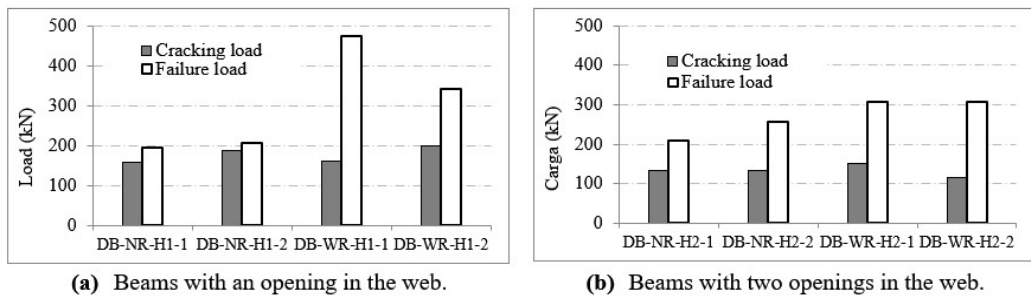(a) Beams with an opening in the web. (b) Beams with two openings in the web.

Figure 8. Comparison between cracking loads and failure loads

3.2 Cracking patterns

Figures 9 to 16 show the cracking patterns of the deep beams, illustrating the development of cracks as the load increases. Cracks in the concrete began to form and propagate when the principal tensile stress caused by the applied load exceeded the concrete's tensile strength.

In most of the beams tested, the first observed cracks were flexural cracks in the upper right corner or along the notch. As the applied load increased, shear cracks appeared. The diagonal cracks also increased and extended towards the loading and support positions, which induced the formation of new diagonal and flexural cracks.

3.2.1 Specimens DB-NR-H1

The failure mechanisms of DB-NR-H1-1 and DB-NR-H1-2 are presented in Figure 9 and Figure 10. They showed the first visible cracks at a load level of 82.09% and 89.57% of the failure load, respectively. The behavior of the beams was brittle, with a mixed failure mode, by shear and anchorage failure. The shear failure was evident with the appearance of diagonal cracks that crossed the openings towards the loading and support point.

It was observed that insufficient anchorage caused longitudinal reinforcement to slip. This type of failure does not occur due to shear force but rather due to failure in the anchorage of the tensioned flange. Although preceded by diagonal cracks, this failure occurred abruptly.
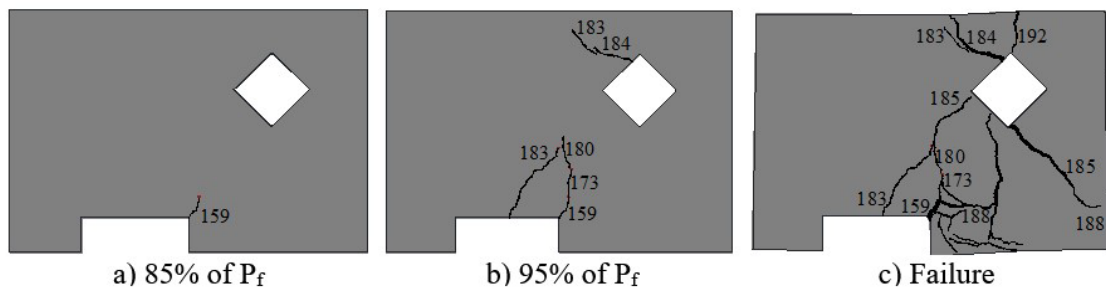

a) 85% of P_f b) 95% of P_f c) Failure

Figure 9. Cracking pattern in DB-NR-H1 (load in kN): (a) 85% of P_f; (b) 95% of P_f; (c) Failure.

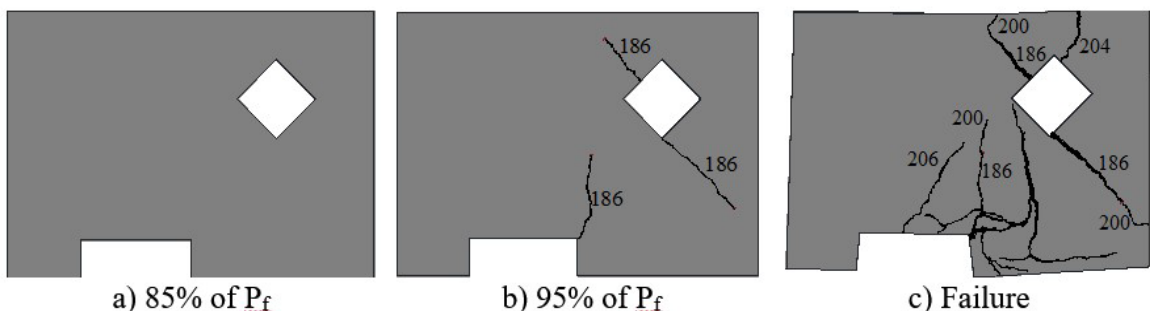a) 85% of P_f b) 95% of P_f c) Failure

Figure 10. Cracking pattern in DB-NR-H1-2 (load in kN): (a) 85% of P_f; (b) 95% of P_f; (c) Failure.

3.2.2 Specimens DB-WR-H1

Beams DB-WR-H1-1 and DB-WR-H1-2 exhibited the first visible cracks at a load level of 33.69% and 58.34% of the failure load, respectively. Similar to other tested beams, cracks were observed in the upper right corner of the notch. Additionally, cracks were also found along the notch and on the right side, caused by flexural and shear effects, extending along the height of the deep beams. Diagonal cracks also appeared, crossing the openings and propagating towards the support and loading point. The failure of the deep beams occurred due to the intensification of flexural cracks along the height, leading to a flexural failure (Figure 11 and Figure 12).

Furthermore, the cracking patterns of DB-NR-H1-1 and DB-NR-H1-2 were similar to those of beams DB-WR-H1-1 and DB-WR-H1-2 with web reinforcement. This behavior is related to the presence of the opening, which partially interfered with the natural path of the loads, altering the distribution of the forces in the section, causing concentration of stresses at the corners of the opening and, consequently, the formation of cracks. An important aspect regarding the existence of asymmetric openings is beam instability. The applied load is carried by two struts, and the absence of either of these struts means that the structure has become unstable.

The use of web reinforcement changed the failure mode of beams without reinforcement from brittle to flexural (ductile). The web reinforcement provided greater plastic strains in the beams, which led to an increase in the cracking pattern.
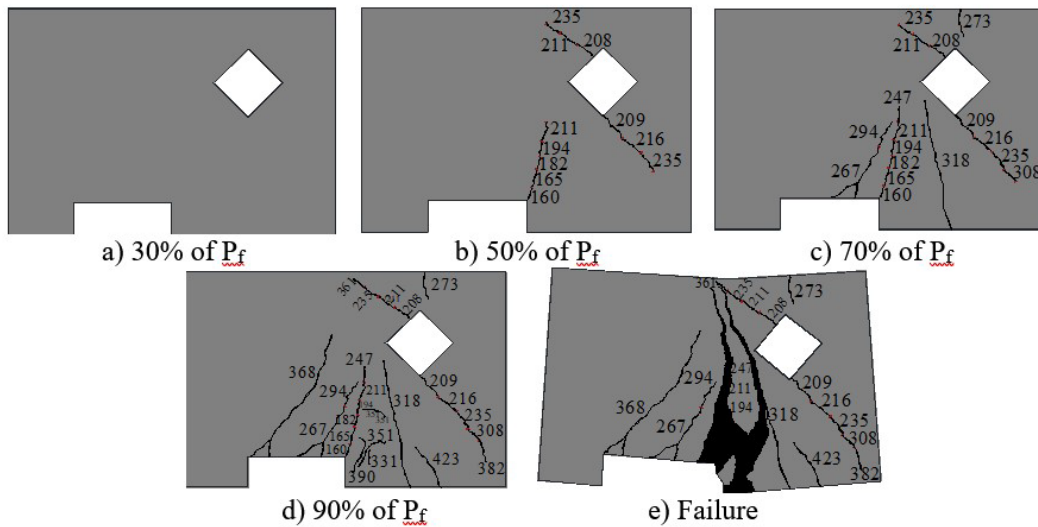

Figure 11. Cracking pattern in DB-WR-H1-1 (load in kN): (a) 30% of P_f; (b) 50% of P_f; (c) 70% of P_f; (d) 90% of P_f; (e) Failure.
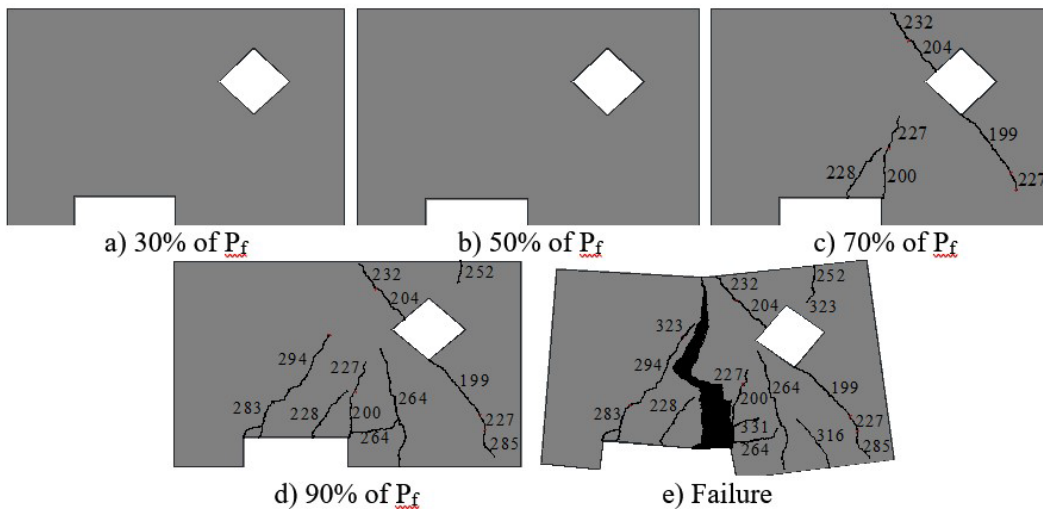

Figure 12. Cracking pattern in DB-WR-H1-2 (load in kN): (a) 30% of P_f; (b) 50% of P_f; (c) 70% of P_f; (d) 90% of P_f; (e) Failure.

3.2.3 Specimens DB-NR-H2

The two DB-NR-H2 beams exhibited comparable crack patterns (see Figure 13 and Figure 14). Prior to failure, they had multiple cracks on the left side, indicating a tendency to form a strut on that side. However, they failed abruptly on the right side. Despite the addition of an extra opening in these beams, they exhibited a failure mechanism on the right side similar to the beams with only one opening.

In DB-NR-H2-1 (Figure 13c), the first visible cracks appeared at 63.30% of the failure load, with a diagonal crack starting on the left side and extending from the upper corner of the opening (diamond) towards the point of loading. The formation of flexural cracks in the lower corner was also observed towards the notch and in the central region of the notch. At load levels of 96.61% and 98.99% of the ultimate load, the shear effect was evident with the appearance of diagonal cracks connecting the load application point to the right support and crossing the opening.

Beam DB-NR-H2-2 presented the first visible cracks at 51.67% of the failure load. This specimen exhibited a flexural crack in the lower corner of the opening, and on the left side of the specimen towards the notch. Additionally, flexural cracks in the central region of the notch were observed, as shown in Figure 14c. At the load level of 55.95% of the failure load, a diagonal crack (shear) was detected, originating from the upper corner of the opening on the left side towards the loading point. Furthermore, it was identified that at 64.11% of the failure load, a crack emerged in the upper right corner of the notch, as observed in the other deep beams.
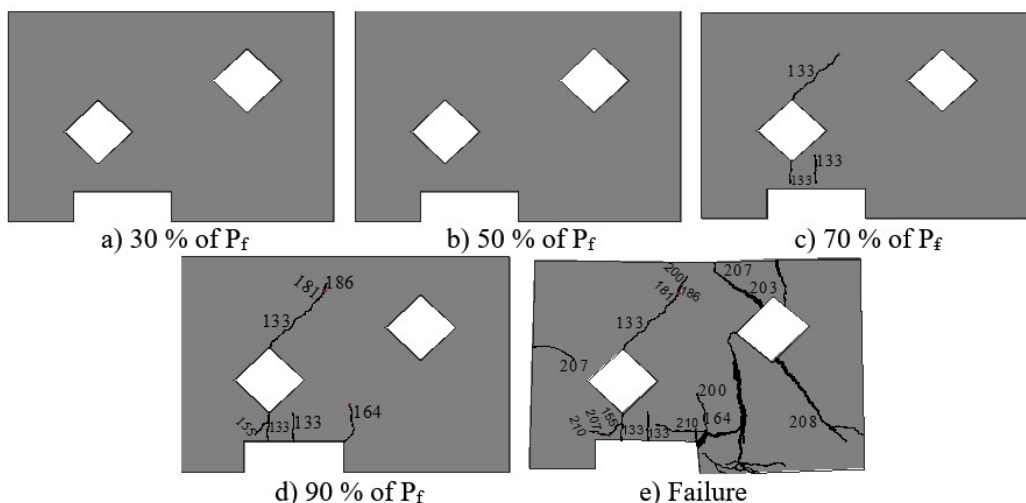

a) 30 % of P$_f$ b) 50 % of P$_f$ c) 70 % of P$_f$

d) 90 % of P$_f$ e) Failure

Figure 13. Cracking pattern in DB-NR-H2-1 (load in kN): (a) 30% of P$_f$; (b) 50% of P$_f$; (c) 70% of P$_f$; (d) 90% of P$_f$; (e) Failure.

a) 30 % of P$_f$ b) 50 % of P$_f$ c) 70 % of P$_f$
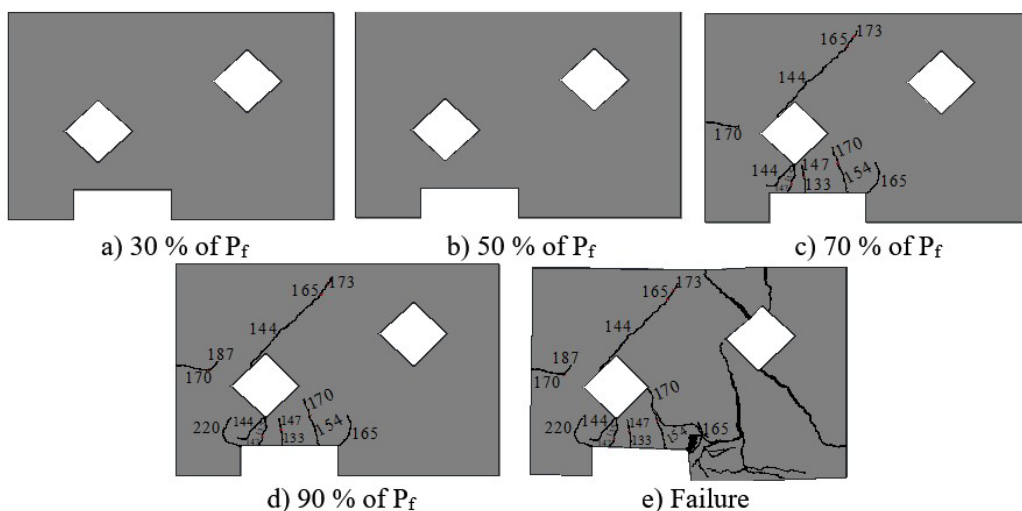
d) 90 % of P$_f$ e) Failure

Figure 14. Cracking pattern in DB-NR-H2-2 (load in kN): (a) 30% of P$_f$; (b) 50% of P$_f$; (c) 70% of P$_f$; (d) 90% of P$_f$; (e) Failure.

For DB-NR-H2-1 and DB-NR-H2-2, failure occurred due to shear and anchorage failure. The longitudinal reinforcements slipped in relation to the concrete, causing separation of the concrete-steel bond. The shear failure mechanism was evident with the appearance of diagonal cracks that crossed the opening, connecting the load application point to the right support. At the moment of failure, these cracks opened significantly due to the absence of reinforcements to absorb the forces.

3.2.4 Specimens DB-WR-H2

The cracking patterns of DB-WR-H2-1 and DB-WR-H2-2 are displayed in Figures 15 and 16, respectively. The first visible cracks appeared at load levels of 49.08% and 37.92% of the failure load, respectively. The cracks were primarily concentrated on the left side until load levels of 250 kN for DB-WR-H2-1 and 187 kN for DB-WR-H2-2. However, due to the redistribution of asymmetric stresses resulting from the asymmetric openings, cracks appeared on the right side. As the loads increased, the cracks widened, and new cracks emerged on the left side. The beams failed due to flexural-shear.
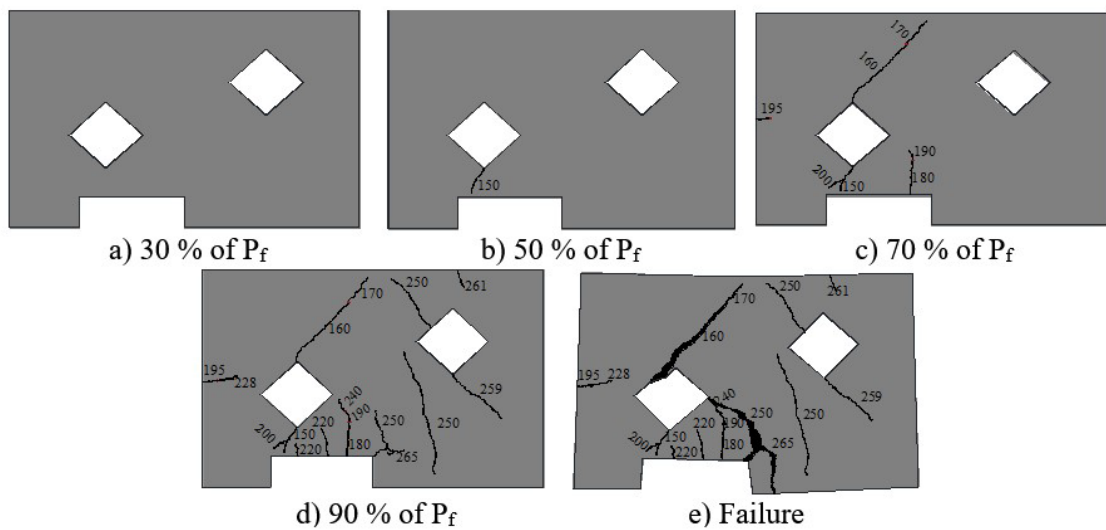

Figure 15. Cracking pattern in DB-WR-H2-1 (load in kN): (a) 30% of P_f; (b) 50% of P_f; (c) 70% of P_f; (d) 90% of P_f; (e) Failure.
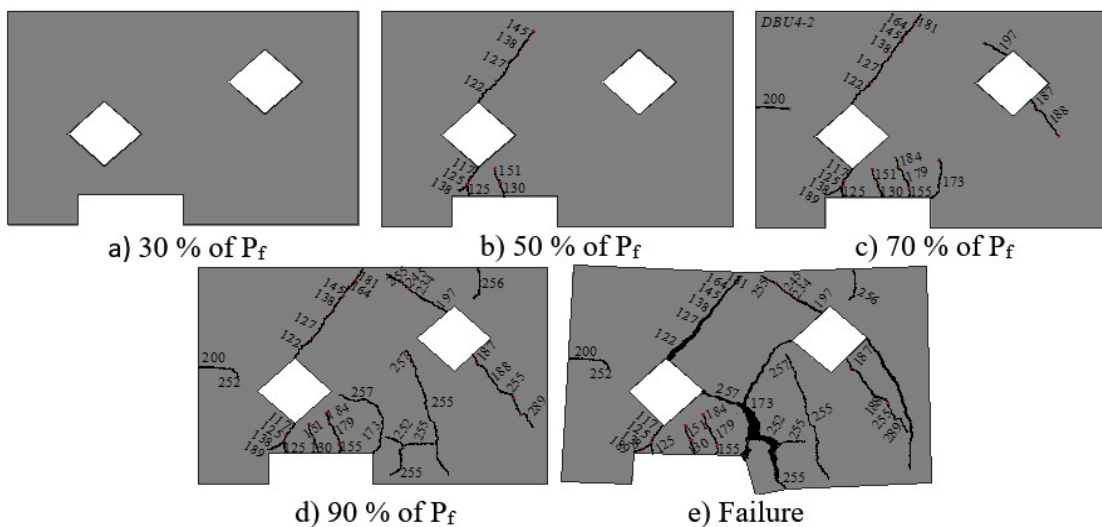

Figure 16. Cracking pattern in DB-WR-H2-NA-2 (load in kN): (a) 30% of P_f; (b) 50% of P_f; (c) 70% of P_f; (d) 90% of P_f; (e) Failure.

Rev. IBRACON Estrut. Mater., vol. 17, no. 6, e17606, 2024

10/21

3.3 Load-strain curves

The load-strain curves for all beams are displayed in Figures 17 to 20. These figures depict the strains of the flexural reinforcement during different loading stages. The graphs also indicate the load level at which the first crack was observed (dashed line) and the initial yield strain of 2.87 ‰, obtained from the steel characterization tests, represented by a vertical line. Regarding the strains of the flexural reinforcements of the tested beams, the results clearly shows that beams with web reinforcement exhibited higher strain than those without it.

For all the beams without web reinforcement, the flexural bars did not reach the yield stress, excluding the possibility of flexural failure, as observed in Figure 17 and Figure 19. The deep beams with web reinforcement presented several disturbances in the flexural bar strains at the second stage (after the appearance of the first crack), resulting from a greater number of crack openings and certain plastic accommodations, which produced stress redistributions along the cracked beams (Figure 18 and Figure 20).
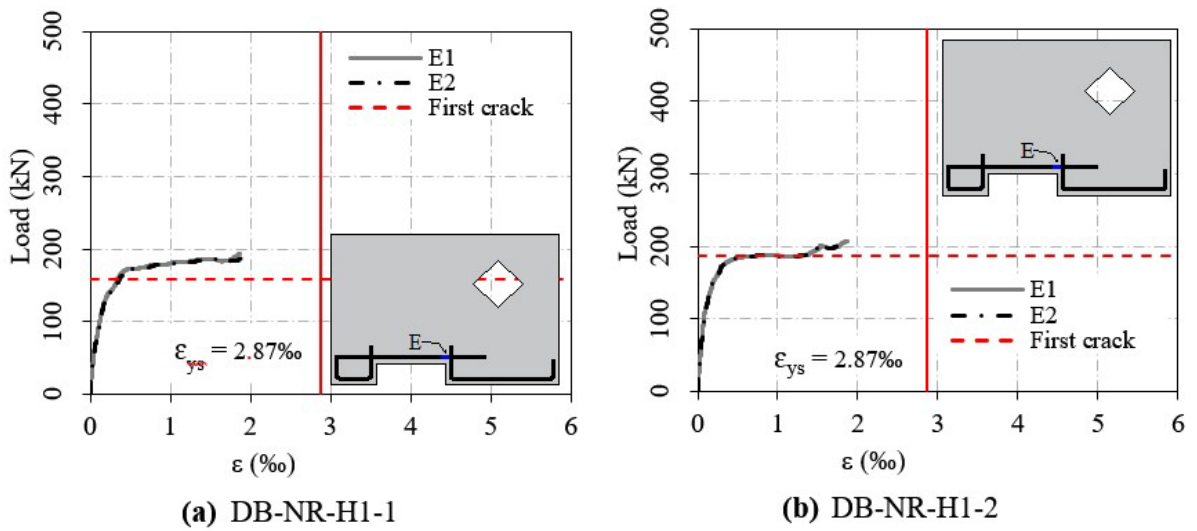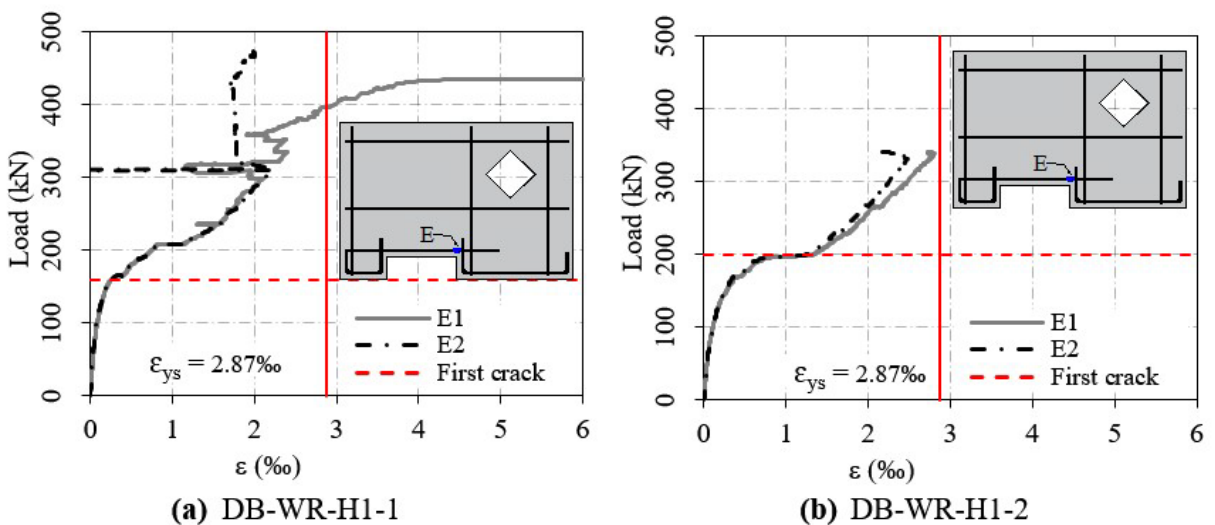

Figure 17. Load-strain curve
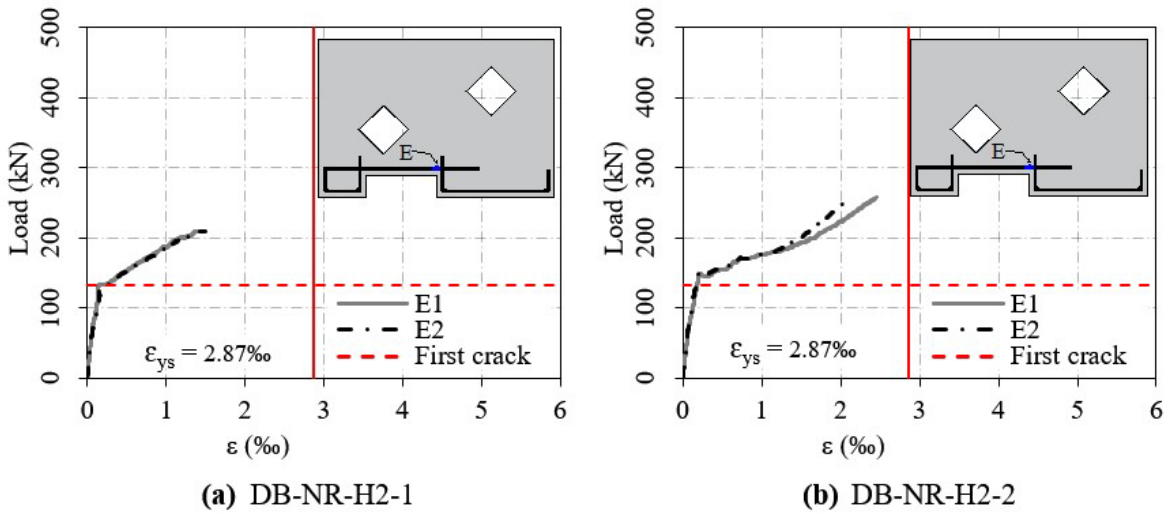

Figure 18. Load-strain curve

Rev. IBRACON Estrut. Mater., vol. 17, no. 6, e17606, 2024

11/21

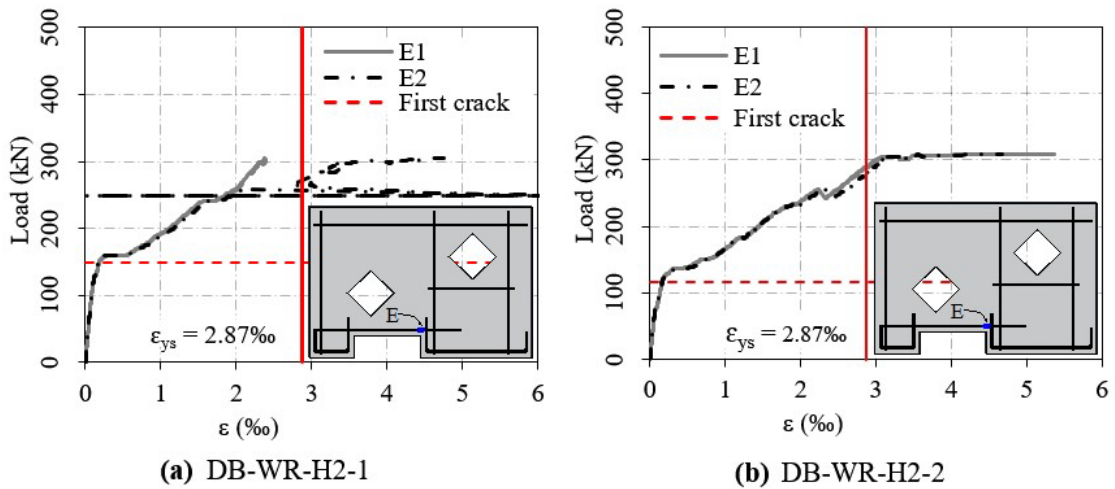**Figure 19.** Load-strain curve

Figure 20. Load-strain curve

4 STRUT-AND-TIE ANALYSIS

A study of strut-and-tie models was carried out for the experimentally tested deep beams. Initially, stress analysis was conducted using the ForcePAD software for the geometries DB-H1 (Figure 1(a)) and DB-H2 (Figure 1(b)). Based on the modeling of the beams, the software can represent all principal stress directions or stresses with specific directions associated with the conditions affecting the software, such as the definition of the element's geometry, the location of loads and supports that the structure is subjected to.

Figures 21 and 22 show the trajectories analysis of the principal tensile and compressive stresses generated by the ForcePAD software for the DB-H1 and DB-H2 geometries, respectively.
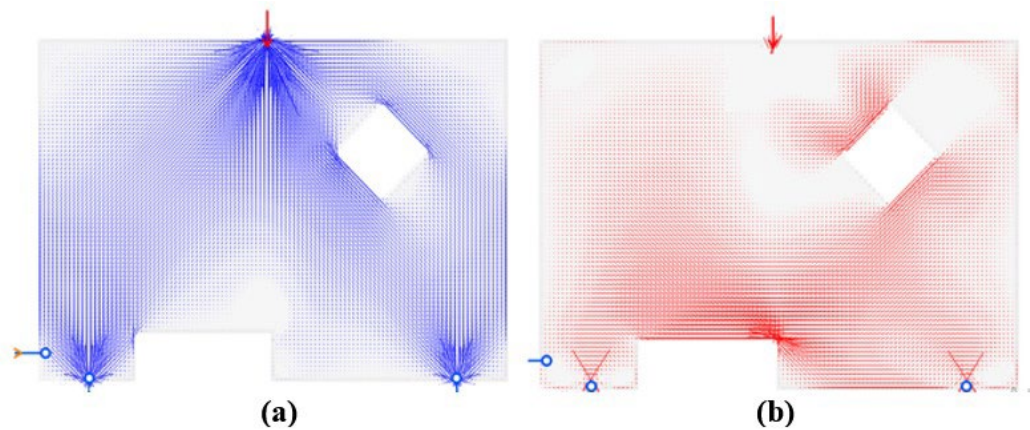
Figure 21. DB-H1 analysis results: **(a)** Principal compressive stress; **(b)** Principal tensile stress.
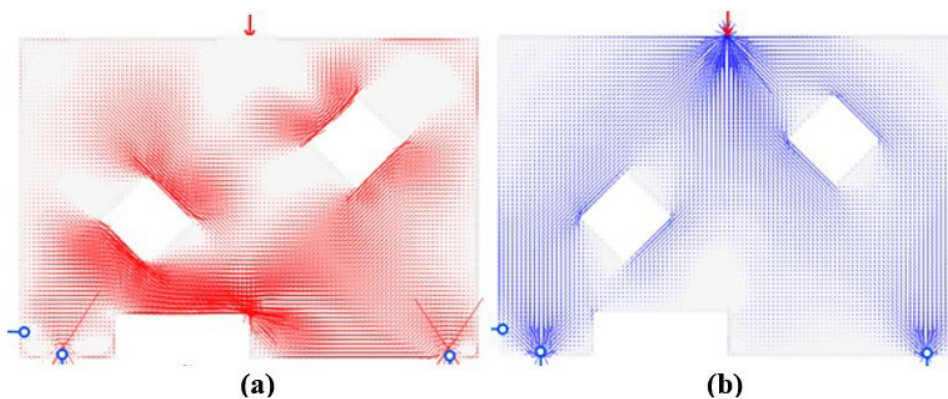

Figure 22. DB-H2 analysis results: **(a)** Principal tensile stress; **(b)** Principal compressive stress.

By analyzing Figure 21, it is possible to verify that there are flexural tensile stresses in the regions above and next to the notch, with the highest stresses present in the upper right corner (Figure 21(b)). It can be observed that on the left side of the model (Figure 21(a)), a large, compressed strut is formed from the loading point to the support. On the right side, the compression stress at the loading point is transferred around the opening and diagonally towards the support. This path of stresses generates, at 45° to the horizontal and parallel to the diamond-shaped opening faces, the formation of struts. At 135° to the horizontal, the formation of ties is also observed.

In Figure 22, it can be seen for the DB-H2 geometry, that the stresses surrounding the new opening generate the formation of ties at a 45° angle with the horizontal on the opening's faces, and the formation of struts on the faces perpendicular to 135° of the opening. The principal tensile stress is also high in the region above the notch and near the left support.

Knowing the compression and tension regions made it possible to determine the locations of the struts and ties. The analysis of the deep beams using the STM was carried out in the CAST (Computer Aided Strut and Tie, 2000) software. The software allows the user to model the structure, define and calculate the internal truss, and verify the struts and nodes. The concrete compressive strength data and mechanical properties of the steel introduced in the software were in accordance with the experimental program. Furthermore, as a prerequisite of design codes, truss models must be exclusively isostatic and self-equilibrated.

In CAST, it is also possible to predict the failure load of the adopted truss and strut model. The software increases the loading so that an unfavorable situation appears for one of the elements or nodal zones of the model. Thus, an estimate of the resistance capacity of the idealized model is obtained.

Santos [38] noted that the angle formed by competing struts and ties at the same node is a limiting factor for the safety and reliability of a nodal region. The smaller the angle, the lower the resistance to compression of the connecting struts. Several regulations and authors provide guidance on allowed ranges for the angle formed between a strut and a tie, as shown in Table 5.

Table 5. Allowed ranges for the angle formed between the compressed diagonals and the longitudinal reinforcement in the STM.

Normative/Author	Angle θ (°)
NBR 6118 [1]	$30° \leq \theta \leq 63°$
EUROCODE 2 [28]	$21° \leq \theta \leq 45°$
ACI 318 [27]	$25° \leq \theta \leq 65°$
Schlaich and Schäfer [39]	$45° \leq \theta \leq 60°$

In this study, the model's definition considered that the angle between truss elements would comply with the limitations imposed by NBR 6118 [1]. Additionally, efforts were made to ensure that the connecting struts were in the compression regions. Regarding the ties, it was sought to ensure that the centroid of the bars coincided with the centroid of the reinforcements to respect the established cover.

The generated models assumed that the struts had a prismatic shape with a constant thickness and that non-hydrostatic stresses could occur in the nodal zones. The resistance of the struts and nodal zones was calculated using equations from NBR 6118 [1], applying average values of concrete resistance. The interfaces of the nodal regions were determined using Equation 1.

$$w_s = w_t . cos\theta + l_b sen\theta \tag{1}$$

Where:

w_s = struts thickness; w_t = thickness of the tie considered at the interface of the nodal zone;

l_b = support thickness; and θ = angle of inclination between connecting struts and ties.

For the ties, it was considered that the steel resisted tensile stresses when positioned in these respective regions. However, in cases where there was no reinforcement in the tie regions (beams without web reinforcement), to maintain the balance between internal and external forces, it was considered that the concrete resisted tensile stresses. In the analysis of concrete ties, direct tensile strength (f_{ct}) was used, which was obtained by converting the indirect tensile strength value ($f_{ct,sp}$) according to NBR 6118 [1]. The cross-sectional areas of the concrete ties were determined by multiplying the beam width by the effective widths of the concrete ties.

For the models, some elements do not receive compression or tension, and thus, are seen as stabilizers. The program automatically recognizes these elements and establishes null force for them.

4.1 Comparison of STM and Experimental Results

4.1.1 DB-NR-H1

In Figure 23, a comparison between the STM and the experimental is presented. Ties T1, T2, and T3 are considered concrete ties. Figure 24 shows the forces acting on each element of the truss. Positive values indicate tension and negative values indicate compression. The values in parentheses show the ratio between the demand on the element and its resistance, that is, the closer this ratio is to 1, the closer the truss element will be to reaching its maximum capacity. The failure of the idealized model of the deep beams occurs for a load of 208.9 KN. In terms of maximum load prediction, the model was satisfactory as it presented results very close to the experimental ones. The difference between the STM and the experimental result was 4.10%.

The concrete tie T3 became the limiting factor of the model's capacity. According to the STM, tie T3 would lead the beam to failure, and based on the cracking patterns of the beams (Figure 25), it can be said that the model is consistent with the behavior observed. It should also be noted that during the experiment, slippage of the reinforcement of tie T5 was observed. Thus, the reinforcement lost its anchorage, causing it to not exhibit the desired behavior. The concrete ties T1 and T2 are under high stress (Figure 24), a behavior similar to the experimental results (Figure 25), as can be seen by the cracks perpendicular to the upper left and lower right interfaces of the openings.
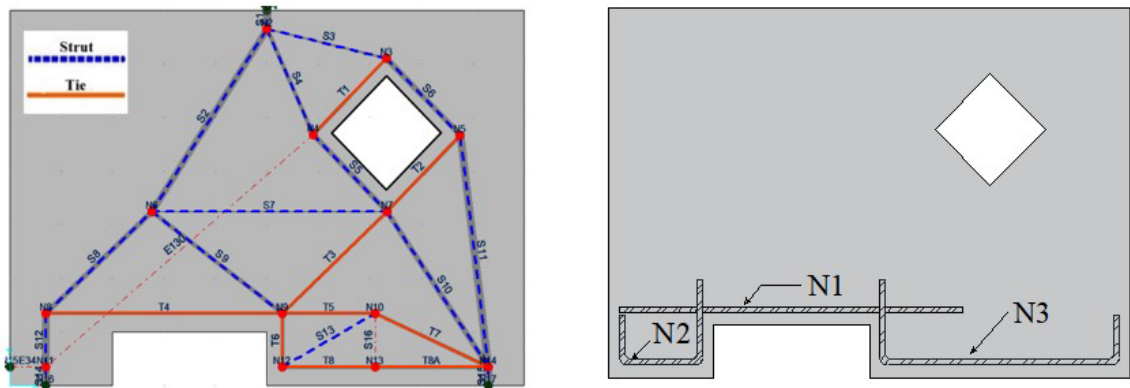
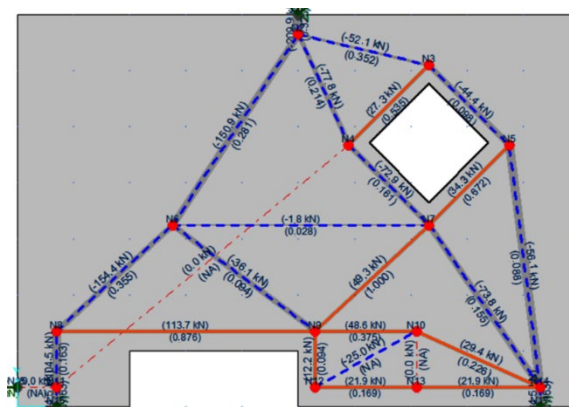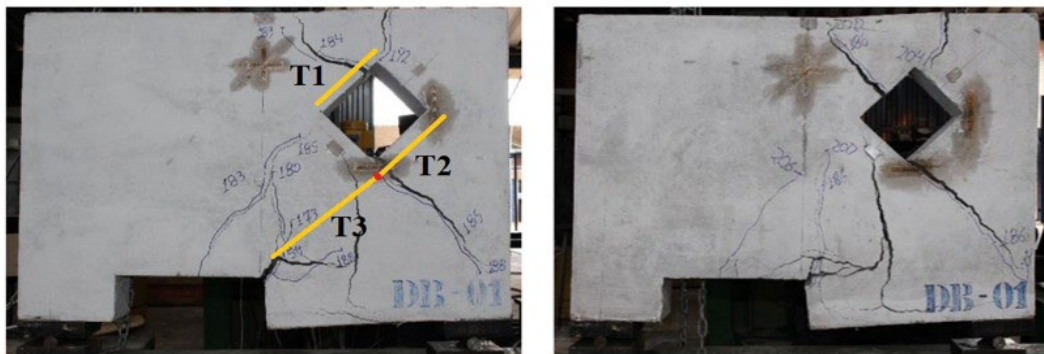**Figure 23.** Comparison between the STM and experimental results

Figure 24. Forces acting on each STM element

a) DB-NR-H1-1   b) DB-NR-H1-2

Figure 25. Failure mode

4.1.2 DB-WR-H1

In Figure 26, a comparison between the STM and experimental results is presented. The forces acting on each truss element are shown in Figure 27. The STM showed a failure load of 312.20 KN. Additionally, the results indicated that the truss elements that reached its maximum resistance capacity was tie T21, T22 and T23.

The model it was able to satisfactorily represent the behavior of the main tensile reinforcements present in the region of ties T21, T22 and T23 at failure, indicating ductile failure (Figure 28). In terms of maximum load prediction, the model underestimated the results obtained in the tests. The difference between the STM and experimental results was -23.48%.
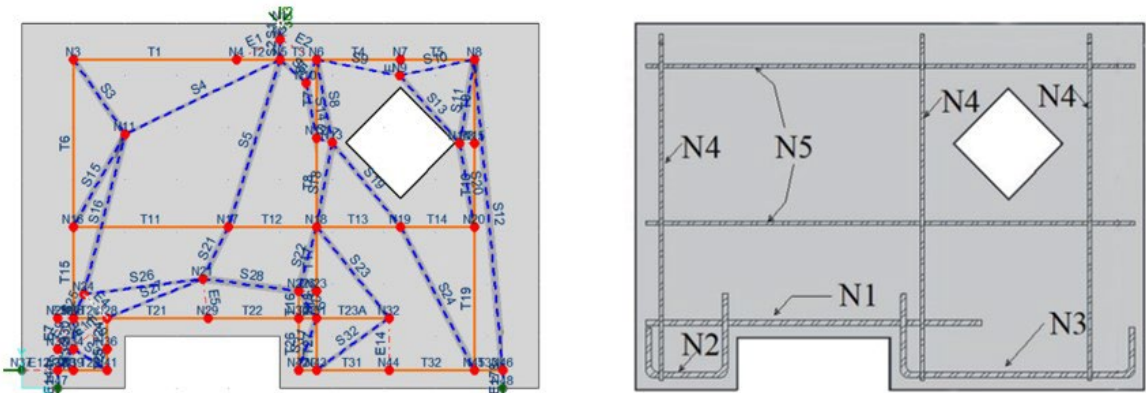
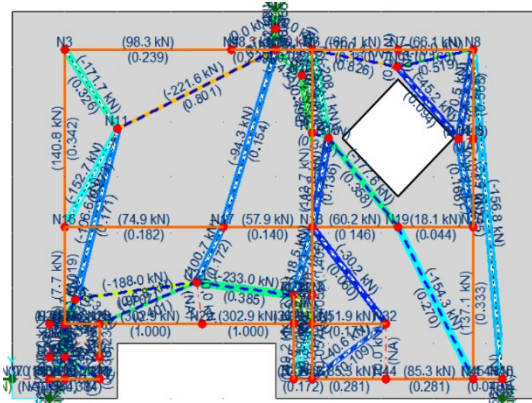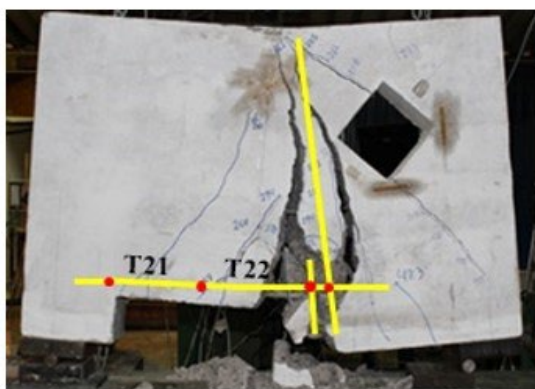**Figure 26.** Comparison between the STM and experimental results.

Figure 27. Forces acting on each STM element.

Based on Figure 28, it is evident that the inclined cracks that are perpendicular to the faces of the openings decreased significantly compared to the DB-NR-H1 beams, owing to the presence of web reinforcement. The main cracks, which indicate the failure mode of the deep beams, started perpendicular to the ties T22 and T23. This kind of crack, which initiates vertically in the lower part of the beam and rises as the load increases, is typical of flexural.

a) DB-WR-H1-1　　　　　　　　　　b) DB-WR-H1-2

Figure 28. Failure mode

4.1.3 DB-NR-H2

In Figure 29, a comparison between the STM and experimental results is presented. T1, T2, T3, T4, and T5 ties are considered concrete ties, while the other ties were modeled as steel ties.
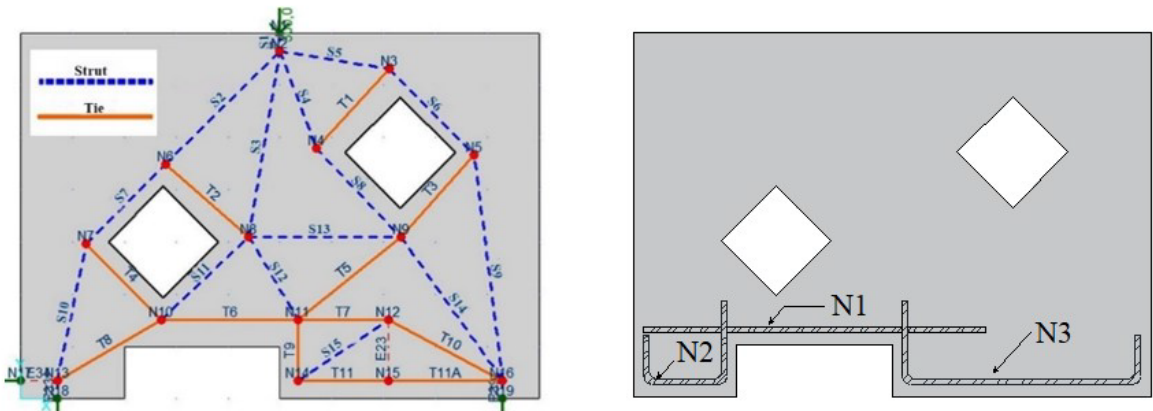

Figure 29. Comparison between the STM and experimental results

The maximum loading capacity of DB-NR-H2 was achieved due to the maximum tensile strength of the concrete tie T4. The maximum load obtained by STM was 161.4 kN. This value is lower than the value found for a similar deep beam with only one opening (208.9 kN). This is attributed to the addition of a new opening, which influenced the path of stresses and, consequently, its load-bearing capacity. The forces acting on each truss element are presented in Figure 30.

The STM presented a conservative failure load prediction, underestimating the results obtained in the tests. The difference between the STM and experimental results was -30.94%.
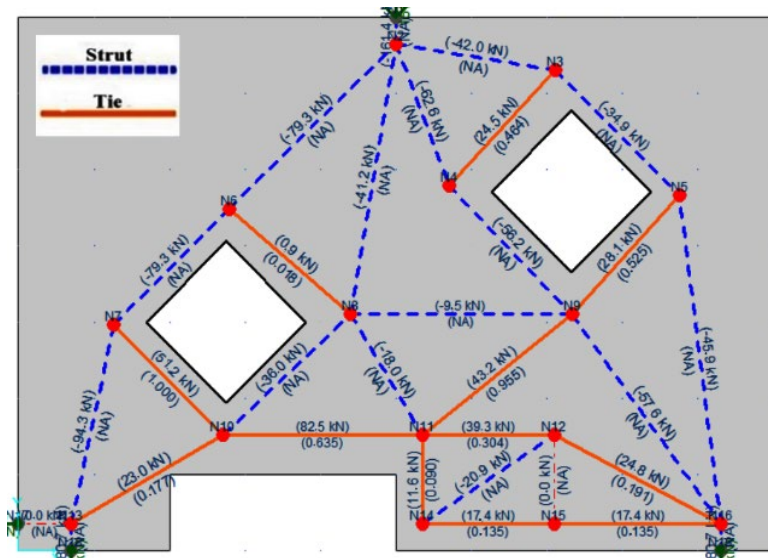

Figure 30. Efforts acting on each element.

The largest cracks are located in the regions of concrete ties T1, T3, and T5 (Figure 31). The cracking clearly shows too the need for steel ties T1, T2, and T3, and the slippage of tie T7. Demonstrating the importance of the presence of steel web reinforcement to absorb shear forces, and the importance of the anchorage of the reinforcement.
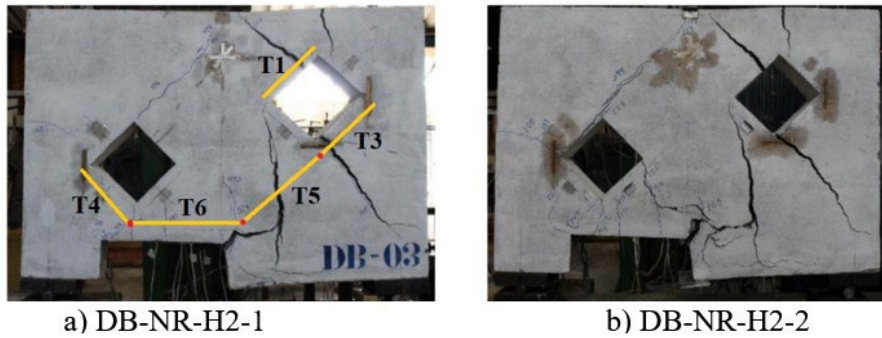
a) DB-NR-H2-1   b) DB-NR-H2-2

Figure 31. Failure mode

According to the STM, the concrete tie T4 would lead the deep beam to failure; however, this behavior was not observed in the tested beams. In the region of tie T4, the formation of cracks is almost nonexistent. This may be attributed to the longitudinal flexural bars, which may have helped absorb tensile forces in that region, or to the lack of symmetry in the application of loading or a flawed design of the STM. However, the most solicited truss elements are precisely the ties that are in the most solicited regions of the deep beams, as shown in the STM.

4.1.4 DB-WR-H2

Figure 32 shows a comparison between the reinforcements of the tested deep beams and the STM. The forces acting on each truss element are shown in Figure 33. Truss elements T22, T23 and T24 was the one that reached its maximum load capacity. The model presented a failure load of 274.30 kN. The difference between the failure load result from the STM and the experimental was -10.67%.
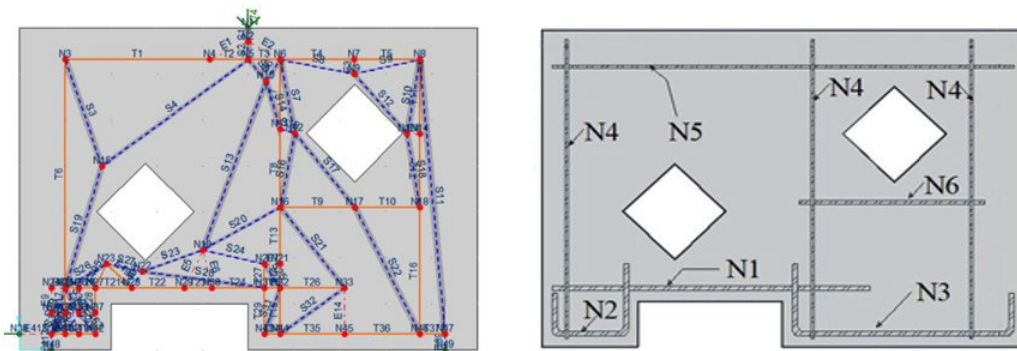

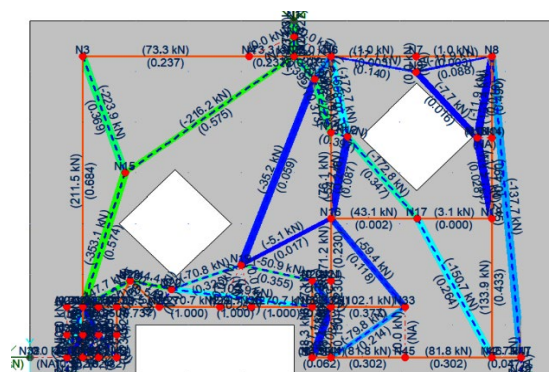**Figure 32.** Comparison between the STM and experimental results

Figure 33. Efforts acting on each element

The model it was able to satisfactorily represent the failure behavior of the main tensile reinforcements present in the region of the T24 tie rod (Figure 33). Furthermore, the experimental results clearly indicate the formation of cracks in this section of the deep beam. (Figure 34).
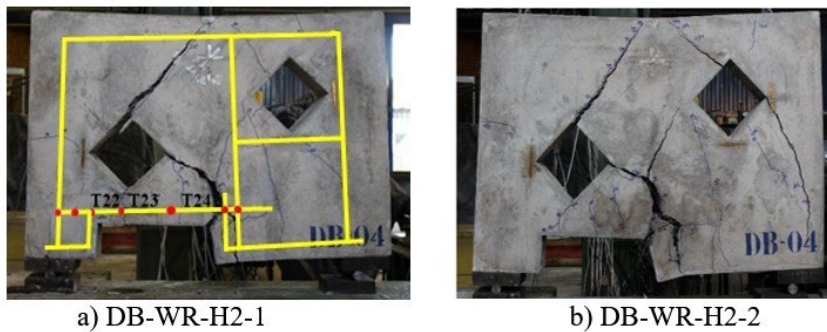

a) DB-WR-H2-1   b) DB-WR-H2-2

Figure 34. Failure mode

5 CONCLUSIONS

This study aimed to experimentally evaluate the behavior of eight deep beams with unconventional geometries containing notches and openings. Additionally, strut-and-tie models were constructed to represent the behavior of the deep beams in terms of failure mode and maximum load. Based on the analysis and discussions presented, it can be concluded that the test configuration used in the experimental study was efficient and presented acceptable behavior. Moreover, all planned parameters could be collected without significant difficulties.

The capacity of deep beams to resist ultimate loads is primarily influenced by the presence of web reinforcement. The inclusion of web reinforcement results in deep beams exhibiting greater resistance, generating a progressive increase in ductility and failure loads. Moreover, it was possible to observe the development of several cracks before the deep beams ultimately failed. This behavior is credited to the vertical shear reinforcements, which can directly absorb a portion of the shear force generated in the beams. When combined with horizontal reinforcements, they promote restraint to the concrete and enable higher resistant stresses to be achieved.

The deep beams with one opening, which had web reinforcement, showed an increase in the average ultimate load of about 103.31% compared to the deep beams without reinforcement in the web. The average ultimate load capacity of the deep beams with two openings, also with web reinforcement, increased by 31.4% compared to the beams without reinforcement in the web. This reinforcement provided a more ductile failure.

The deep beams without web reinforcement exhibited higher ratios between cracking and failure loads than those with web reinforcement.

The failure modes predicted by the STM were consistent with the experimental tests. The regions in which the truss elements were more solicited were similar to the tested models. Regarding the ultimate loads that led the deep beams to failure, the STM predicted lower resistances than the experimental data (average values) by 23.48%, 30.94%, and 10.67% for DB-WR-H1, DB-NR-H2, and DB-WR-H2, respectively. For DB-NR-H1, the STM predicted a value close to the experimental, with a difference of 4.10%. Most of the failure load results showed that the STM is conservative.

6 ACKNOWLEDGEMENTS

7 REFERENCES

[1]   Associação Brasileira de Normas Técnicas, *Design of concrete structures - procedure*, NBR 6118, 2014.

[2]   F. K. Kong and M. Chemrouk, "Reinforced concrete deep beams," in *Reinforced concrete deep beams*, F. K. Kong, Ed., Nova York: Van Nostrand Reinhold, 2002, pp. 17–36.

[3] G. Russo, R. Venir, and M. Pauletta, "Reinforced concrete deep beams - shear strength model and design formula," *ACI Struct. J.*, vol. 102, pp. 429–437, 2005.

[4] T. El-Maaddawy and B. El-Ariss, "Behavior of concrete beams with short shear span and web opening strengthened in shear with CFRP composites," *J. Compos. Constr.*, vol. 16, pp. 47–59, 2012.

[5] F. K. Kong and G. R. Sharp, "Shear strength of lightweight reinforced concrete deep beams with web openings," *Inst. Struct. Eng*, vol. 51, pp. 267–275, 1973.

[6] M. A. Mansur and W. A. Alwis, "Reinforced fibre concrete deep beams with web openings," *Int. J. Cement. Compos. Light Concr*, vol. 6, pp. 263–271, 1984.

[7] N. E. Shanmugam and S. Swaddiwudhipong, "Strength of fibre reinforced concrete deep beams containing openings," *Int. J. Cement. Compos. Light Concr*, vol. 10, pp. 53–60, 1988.

[8] K. H. Yang, H. C. Eun, and H. S. Chung, "The influence of web openings on the structural behavior of reinforced high-strength concrete deep beams," *Eng. Struct.*, vol. 28, pp. 1825–1834, 2006.

[9] K. H. Tan and O. E. Hu, "Large reinforced-concrete deep beams with web openings: Test and strut-and-tie results," *Mag. Concr. Res.*, vol. 59, pp. 423–434, 2007.

[10] M. F. Andermatt and A. S. Lubell, "Behavior of concrete deep beams reinforced with internal fiber-reinforced polymer – Experimental study," *ACI Struct. J.*, vol. 110, no. 4, pp. 585–594, 2013.

[11] S. C. Chin and S. I. Doh, "Behaviour of reinforced concrete deep beams with openings in the shear zones," *J. Eng. Technol.*, vol. 6, no. 1, pp. 60–71, 2015.

[12] F. K. Kong and G. R. Sharp, "Structural idealization for deep beams with web openings," *Mag. Concr. Res.*, vol. 29, pp. 81–91, 1977.

[13] A. F. Ashour and G. Rishi, "Tests of reinforced concrete continuous deep beams with web openings," *ACI Struct. J.*, vol. 97, pp. 418–426, 2000.

[14] A. F. Ashour and G. Rishi, "Tests of reinforced concrete continuous deep beams with web openings," *ACI Struct. J.*, vol. 97, pp. 418–426, 2000.

[15] K. H. Yang and A. F. Ashour, "Structural behaviour of reinforced-concrete continuous deep beams with web openings," *Mag. Concr. Res.*, vol. 59, pp. 699–711, 2007.

[16] T. E. Maaddawy and S. Sherif, "FRP composites for shear strengthening of reinforced concrete deep beams with openings," *Comp. Struct*, vol. 89, pp. 60–69, 2009.

[17] G. Campione and G. Minafo, "Behaviour of concrete deep beams with openings and low shear span-to-depth ratio," *Eng. Struct.*, vol. 41, pp. 294–306, 2012.

[18] D. R. Sahoo, C. A. Flores, and S. H. Chao, "Behavior of steel fiber-reinforced concrete deep beams with large opening," *ACI Struct. J.*, vol. 109, pp. 193–204, 2012.

[19] N. R. B. Yahya, "Effects of square openings in reinforced concrete deep beams," M. S. thesis, University Malaysia Pahang, Pahang, Malaysia, 2014.

[20] C. C. Tseng, S. J. Hwang, and W. Y. Lu, "Shear strength prediction of reinforced concrete deep beams with web openings," *ACI Struct. J.*, vol. 114, pp. 1569–1579, 2017.

[21] A. A. Vieira, "Experimental and numerical analyses of reinforced concrete deep beams with unconventional geometries," M. S. thesis, UNB, Brasília, Brasil, 2018.

[22] W. A. Jasim, A. A. Allawi, and N. K. Ali Oukaili, "Effect of size and location of square web openings on the entire behavior of reinforced concrete deep beams," *Civ. Eng. J.*, vol. 5, no. 1, pp. 209, 2019.

[23] S. A. Hassan and M. K. Ali, "Effect of web Opening shape on the behavior of the hybrid reinforced concrete beam under repeated loading," *J. Eng. Sust. Dev.*, vol. 23, no. 03, pp. 128–141, 2019.

[24] A. H. Abdel-Kareem and I. A. El-Azab, "Behavior of concrete deep beams reinforced with inclined web reinforcement around different opening shapes," *Adv. Res.*, vol. 20, pp. 1–12, 2019.

[25] A. Kumari and A. N. Nayak, "An experimental approach for strengthening of RC deep beams with web openings using GFRP fabrics and gas actuated fasteners," *J. Build. Eng.*, vol. 35, pp. 102027, 2021.

[26] M. T. Ley, K. A. Riding, and S. Windianto, "Bae, and J. E. Breen. Experimental Verification of Strut-and-Tie Model Design Method," *ACI Struct. J.*, no. 104, pp. 749–755, 2007.

[27] American Concrete Institute, *Building Code Requirements for Structural Concrete*, ACI 318, 2019.

[28] European Committee for Standardization, *Eurocode 2: Design of Concrete Structures Part 1-1: General Rules and Rules for Buildings*, EN 1992-1-1, 2004.

[29] Fib Bulletin, *Model Code 2010: First Complete Draft. FIB Bulletin 55*. Lausanne, Suiça: CEB-FIP.

[30] J. Schlaich, K. Schafer, and M. Jennewein, "Toward a consistent design of structural concrete," *J. Prestressed Concr. Inst.*, vol. 32, pp. 74–150, 1987.

[31] E. Mörsch, *Concrete-steel construction*. New York, U.S.: The Engineering News Publishing Company, 1909.

[32] W. Ritter, "Die bauweise hennebique," *Schweiz. Bauzeitung*, vol. 33, no. 7, pp. 59–61, 1899.

[33] S. Fan, Y. Zhang, Y. X. Ma, and K. H. Tan, "Strut-and-tie and finite element modelling of unsymmetrically-loaded deep beams," *Struct.*, vol. 36, pp. 805–821, 2022.

[34] Associação Brasileira de Normas Técnicas, *Concrete - Procedure for molding and curing specimens*, NBR 5738, 2008.

[35] Associação Brasileira de Normas Técnicas, *Concrete - Compression test of cylindrical specimens*, NBR 5739, 2007.

[36] Associação Brasileira de Normas Técnicas, *Mortar and concrete - Determination of the tensile strength by diametrical compression of cylindrical specimens*, NBR 7222, 2011.

[37] Associação Brasileira de Normas Técnicas, *Metallic materials - Tensile test at room temperature*, NBR 6892, 2013.

[38] D. D. Santos, "Análise de vigas de concreto armado utilizando modelos de bielas e tirantes," M. S. thesis, EESC USP, São Carlos, 2006.

[39] J. Schlaich and K. Schäfer, "Design and detailing of structural concrete using strut-and-tie models," *The Struct. Eng.*, vol. 32, pp. 133–125, 1991.

Rev. IBRACON Estrut. Mater., vol. 17, no. 6, e17606, 2024

21/21